Available online at www.sciencedirect.com

ScienceDirect

journal homepage: www.elsevier.com/locate/he

Effect of $NaBF_4$ addition on the anodic synthesis of TiO_2 nanotube arrays photocatalyst for production of hydrogen from glycerol–water solution

Ratnawati [a,c], *Jarnuzi Gunlazuardi* [b], *Eniya Listiani Dewi* [d], *Slamet* [a,*]

[a] *Department of Chemical Engineering, Faculty of Engineering, Universitas Indonesia, Depok 16424, Indonesia*
[b] *Department of Chemistry, Universitas Indonesia, Depok 16424, Indonesia*
[c] *Department of Chemical Engineering, Institut Teknologi Indonesia, Tangerang Selatan 15320, Indonesia*
[d] *Agency for the Assessment and Application Technology, Puspiptek, Serpong, Tangerang Selatan 15320, Indonesia*

ARTICLE INFO

Article history:
Received 22 April 2014
Received in revised form
18 July 2014
Accepted 30 July 2014
Available online 5 September 2014

Keywords:
TiO_2 nanotube arrays
Anodic oxidation
Photocatalytic
Hydrogen

ABSTRACT

Addition of $NaBF_4$ during anodic synthesis of TiO_2 nanotube arrays (TNTAs) photocatalyst and its application for generating hydrogen from glycerol–water solution has been investigated. The TNTAs were synthesized by anodic oxidation of titanium metal in glycerol electrolyte solution containing NH_4F. During the process, the $NaBF_4$ with different concentrations were added to the solution. Annealing of the formatted TNTAs were performed at 500 °C for 3 h under 20% H_2 in argon atmosphere, to produce crystalline phase photocatalyst. FESEM analysis showed that self-organized and well ordered TNTAs have range of inner diameters, wall thicknesses and lengths approximately 62–130 nm, 27 nm and 1.53 μm, respectively. FTIR analysis indicated that carbon, nitrogen and boron were incorporated into the TNTAs lattice. Refer to UV–Vis DRS and XRD analysis, the TNTAs photocatalysts prepared have the band gap range of 2.70–3.10 eV, with mostly have anatase phase. The $NaBF_4$ addition during synthesis, resulted modified TNTAs that can reduce the recombination of photo-induced electrons-holes. Photocatalytic hydrogen production test, from glycerol–water solution, indicated that TNTAs with the addition of $NaBF_4$ during anodic synthesis process showed higher hydrogen production comparing to the one without $NaBF_4$ addition. Among them the TNTAs,b (with the addition 5 mM of $NaBF_4$) showed up to 32% improvement in the hydrogen production and can be considered as the optimum condition.

Introduction

Hydrogen as renewable and clean energy which provides zero emission of pollutants is necessary to be concerned due to increasing global energy demand [1], inevitable depletion of fossil fuels and environmental issues [2]. To produce H_2, the traditional technologies such as steam reforming and pyrolysis have some obstacles e.g. massive energy consumption, pure oxygen requirement and suffering from H_2 selectivity [3]. The photocatalytic splitting of water over TiO_2 for H_2 production has been considered as a promising alternative

* *Corresponding author*. Tel.: +62 021 7863516; fax: +62 021 7863515.
E-mail address: slamet@che.ui.ac.id (Slamet).
http://dx.doi.org/10.1016/j.ijhydene.2014.07.178

technology [2,4]. Since its application in fuel cells gives high-energy efficiency, it has received much attention indicated by high demand in the market [5]. On the other hand, biomass-derived waste such as glycerol solution (by-product of the biodiesel industry that now has limited demand in the market) [6], presents a particularly attractive renewable and sustainable source for H_2 generation. Glycerol solution gives some advantages since glycerol serves as a hydrogen source, and as a sacrificial agents/electron donor in water splitting, which can increase the H_2 produced from both kinetic and thermodynamic points of view [7]. Therefore, this would be beneficial as a new avenue for the production of H_2 and waste minimization. TiO_2 is the most promising photocatalyst due to its photostability, environmental harmlessness [1,2], availability and relatively inexpensive [2]. Activation of this photocatalyst needs photon energy, which can be provided by solar light at ambient condition instead of thermal energy [3]. TiO_2 has many applications such as photocatalyst in H_2 generation [1–4,6–8], pollutant degradation [9,10], dye-sensitized solar cells [11], and it is commonly used as a semiconductor in photo-spitting of water. In this photo-splitting, TiO_2 has suitable valence and conduction band position for reduction of H^+ and oxidation of OH^- [4,12]. However, the application of TiO_2 has several drawbacks in term of photoinduced electron–hole recombination [2,4], limited surface area and visible light inactive (its wide band gap i.e. 3.2 eV for the anatase and 3.0 eV for rutile phase) [13,14]. Consequently, its utilization efficiency especially in solar light is still poor as UV portion accounts for only about 5%, meanwhile visible light accounts for about 45% in solar spectra [13,14]. Therefore, some modifications strategies need to be executed to reduce those drawbacks such as morphology modifications [1–4,7–14], non-metal (C, N, B) and metal (Pt, Cu) doping [2–4,6–12,14], coupling with other semiconductors such as CdS [15] and addition of sacrificial agent such as methanol, ethanol, propanol and glycerol [2–7,12].

Extensive efforts have been performed to enhance photoactivity of TiO_2 by synthesizing it to get morphology modifications in the forms of nanotubes, nanowire and nanorod [1–4,10–20]. It was reported that TiO_2 nanotube arrays (TNTAs) morphology, obtaining by anodic process of titanium metal, has performed better properties as it provides a larger surface area and superior performance in charge transport than other morphologies [13,14,16–20]. In addition, modification of TNTAs by using dopant materials can improve their activity under visible light illumination [10,11,16–20]. When TNTAs synthesized in organic electrolyte such as glycerol containing ammonium fluoride (NH_4F) and followed by addition of $NaBF_4$ in the electrolyte solution, not only longer TNTAs can be produced [16], but may also lead to the incorporation of dopant C, N, F, and B in the lattice of TNTAs. This is because, those precursors (glycerol, NH_4F and $NaBF_4$) are already available in the electrolyte solution along the process [10,19,21]. This simple method (in-situ co-doping of C, N, F and B) resulted in better quality nanotubes than the post-treatment method. In recent years, anionic doped (C, N) into TNTAs had been studied intensively for photocatalytic H_2 production and waste degradation [14,16–19]. Boron doped into TNTAs is also used to degrade pollutant [10,16,20] and dye-sensitized solar cells [11]. The incorporating boron to the TNTAs lattice can occur easily as the smaller radius of boron than other non-metals [10]. Furthermore, boron doped to the TNTAs can suppress recombination of photo-induced electrons-holes [9]. However, little attention was paid and detailed studies were absent in respect to the $NaBF_4$ addition in the electrolyte solution to get C, N, F and B co-doped TNTAs via in-situ or one pot anodic oxidation reaction (as a simple method) and its application in H_2 production from glycerol solution (glycerol–water mixture).

In this study, the investigation of C, N, F and B co-doped TNTAs synthesized via in-situ anodic oxidation and its activity under visible light illumination in producing H_2 from photo-reforming of glycerol solution (10 vol% of glycerol) was performed. The TNTAs characterizations were performed by mean FESEM, EDAX, FTIR, UV–Vis DRS, XRD and photocurrent density. Based on these characterizations, the roles of specific parameters in producing hydrogen were examined.

Experimental

Preparation of photocatalyst

Titanium foils (0.3 mm thick, 99.6% purity) were supplied by Baoji Jinsheng Metal Material Co. Ltd. In order to provide a flat surface, the Ti sheets (3 cm × 2 cm) were firstly polished with a 1500 cc sandpaper. Subsequently, Ti samples were degreased in a mixture of HF, HNO_3 and H_2O with a volume ratio of 1:3:6 for 2 min, rinsed in deionized water and dried under air. Anodic oxidation of Ti foils (Ti as an anode and platinum, Pt with thickness 1 mm; area (3 × 1.5) cm^2 as a cathode) was performed at room temperature in 60 ml of electrolyte solution containing 0.5 wt.% NH_4F (Merck, 98%) and 25 v% H_2O in glycerol solution (from Brataco). The space between the two electrodes was maintained at 3.5 cm in all studies. This distance is selected by considering the reactor size and morphology of TNTAs that will be produced [22]. A constant 30 V potential difference was set using DC power supply (Escord 6030SD) for 2 h. This equipment also measured the variation of current generated as a function of time. The selection of constant parameters such as voltage, water content, amount of NH_4F, time and annealing temperature is based on the optimal condition as suggested by previous studies [23]. Magnetically stirring (150 rpm) was done in the anodic oxidation process to homogenize the electrolyte solution in order to get TNTAs with uniform size and to enhance the mobility of the ions inside the solution. The TNTAs was then washed in distilled water and dried under ambient atmosphere. To study the effect of $NaBF_4$ addition in the synthesis of TNTAs, different concentrations of 2.5, 5.0 and 7.5 mM $NaBF_4$ (Merck, 98%) were added to the electrolyte solution (denoted as TNTAs,**a**, TNTAs,**b** and TNTAs,**c**, respectively). All photocatalysts were then underwent annealing under 20% H_2 in argon atmosphere (150 ml s^{-1}) at 500 °C for 3 h with heating rate of 9.2 °C min^{-1} and natural cooling. This annealing condition is considered sufficient to convert the amorphous to anatase phase of TNTAs. Furthermore, this 20% H_2 also helps in suppressing the oxidation reaction of elements (C, N, F and B) that present in synthesized TNTAs and contributes in doping process [14,23].

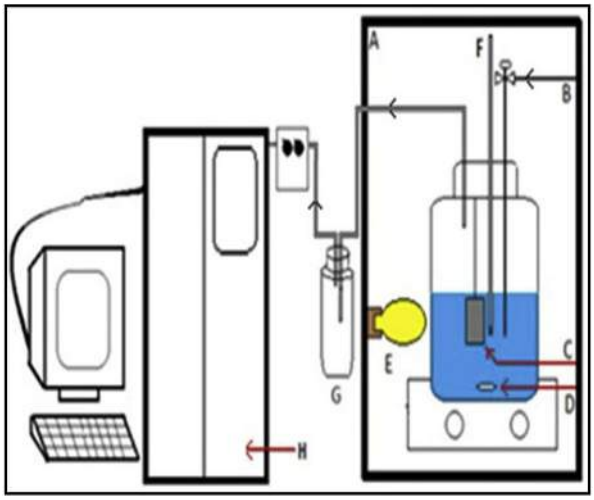

Fig. 1 – Schematic diagram of the photocatalytic reactor: (A) reflector box, (B) line purging, (C) photocatalyst, (D) magnetic stirrer, (E) mercury lamp, (F) thermocouple, (G) liquid condensation tube and (H) GC.

Characterization of photocatalyst

The surface morphology of photocatalyst was examined using an FESEM (FEI-Inspect F50). To determine the elements that present in the photocatalyst, energy dispersive X-ray spectroscopy (EDAX) is attached to the FESEM. To study the functional groups available in the photocatalyst, FTIR analysis (Shimadzu IR Prestige-21) was performed over a wavenumber range of 400–4000 cm^{-1}. To evaluate the effect of NaBF4 addition to the energy band gap of the photocatalyst samples, a UV–Vis DRS analysis was employed using Spectrophotometer Shimadzu 2450 type and the absorbance and reflectance of the samples were recorded under ambient condition in the wavelength range of 200–600 nm. X-ray diffraction (XRD), Shimadzu XRD 7000 X-ray diffractometer, was used to assess the photocatalyst crystalline phases. The source of the X-ray radiation was Cu Kα ($\lambda = 0.154184$ nm), and the scan rate was set $2^{\circ}min^{-1}$ over the 2θ range of 10–80°. The XRD was operated at 40 kV and 30 mA. The crystallite sizes of the photocatalyst were estimated from FWHM (full-width at half-maximum) of XRD according to the Scherrer equation.

Photoelectrochemical test of photocatalyst

Photocurrent was measured in the photoelectrocatalytic reactor with a standard three-electrode configuration, which was connected to a computer - controlled potentiostat (e-DAQ/e-corder 401) to record the generated photocurrent. The each sample (photoanode) was placed as working electrode, while a Pt wire and a saturated Ag/AgCl was placed as counter and reference electrode, respectively. The supporting electrolyte was 0.1 M $NaNO_3$. The reactor, which consisted of a quartz cell with the dimension of 25 mm in diameter, 40 mm in height, and an effective volume of 20 ml was placed in the faraday cage. The samples were illuminated with UV (an 11 W UV lamp/black light, 365 nm) and visible light (a 75 W tungsten lamp, 350–800 nm). The potential was swept linearly at a scan rate of 100 mV/s under illumination.

Photocatalyst test for hydrogen production

All photocatalysts (3 cm × 3 cm) were evaluated for producing H_2 from the reactant (200 ml of glycerol-demineralized water mixture, with 10 v% glycerol) via photocatalysis reaction. The reaction was carried out in a 500 ml Pyrex glass reactor equipped with a mercury lamp of Philips HPL-N 250 W/542 E40 HG ISL as a photon source (17% of UV and 83% of visible light), thermocouple and magnetic stirrer to mix the reactant. The lamp was positioned one cm away from the reactor as a photon source to trigger the photocatalytic reaction. The photoreactor system was placed inside a reflector box, and the reactions were carried out for 4 h irradiation as shown in Fig. 1. Prior to irradiation, reactor was purged by argon to eliminate air for not affecting during H_2 production and to test the leakage of the reactor. The H_2 produced was analyzed by on-line sampling every 30 min using Shimadzu Gas Chromatograph (GC 2014). Molecular sieve (MS Hydrogen 5A, 80–100 mesh) column and CO_2 Parapack N column were used for H_2 and CO_2 analysis, respectively. Thermal Conductivity Detector (TCD) was used to record the signal/peak of H_2 and CO_2 produced. This GC system can detect the area of H_2 and

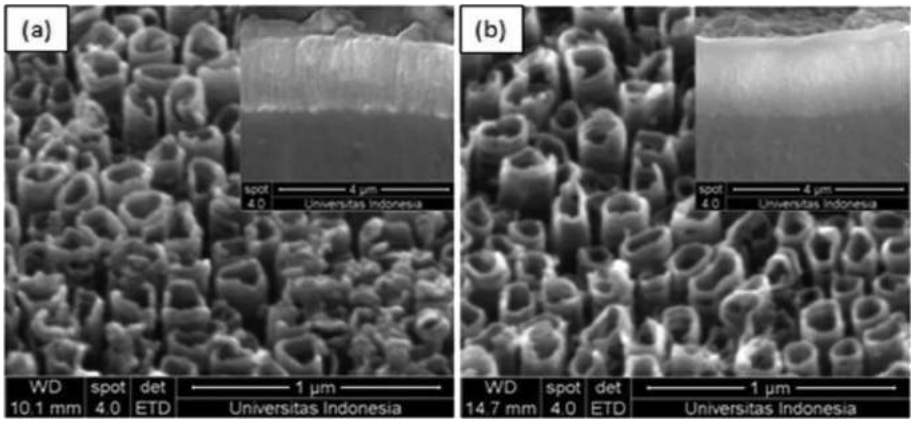

Fig. 2 – FESEM top view image with angle 45° of (a) TNTAs, and (b) TNTAs,c. The inset shows the cross section image with magnification 100 000×.

CO_2 peaks below 50 counts, and it is equipped with GC solution software. High purity argon (99.99%) is used as a carrier gas at 50 cm^3/min.

Results and discussion

FESEM analysis

Fig. 2 depicts FESEM top view image with angle 45° of TNTAs and TNTAs,**c**. The results clearly show that the morphology of TNTAs remains unchanged after $NaBF_4$ addition, in fact the nanotubular structure morphology remains observed in TNTAs,**c** sample. The cross section view image of the photocatalyst samples (inset in Fig. 2) indicates that the self-organized and ordered nanotube arrays are perpendicular to the Ti substrate. It is also found for TNTAs,**a** and TNTAs,**b** (figures not shown). The simultaneous processes of chemical oxidation of Ti metal to TiO_2 in the metal surface and the formation of small pits or tube (chemical dissolution of TiO_2 due to F^- ions from NH_4F) resulted in the formation of TNTAs [16,17]. Those two processes can be represented in the following reactions:

$$Ti + 2H_2O \rightarrow TiO_2 + 4H^+ + 4e^- \quad (1)$$

$$TiO_2 + 6F^- + 4H^+ \rightarrow [TiF_6]^{2-} + 2H_2O \quad (2)$$

With the increasing certain anodization time, the tube length becomes longer. The morphology dimensions of photocatalysts are shown in Table 1, and the distribution of the inner diameter ranges is presented in Fig. 3. As shown in Fig. 3, the TNTAs,**b** has a higher percentage of small size distribution in inner diameter of the nanotubes than other photocatalysts. In contrast, Su et al. [20] reported that B-doped into TNTAs via chemical vapor deposition with boric acid underwent disintegration of morphological integrity. Refer to Fig. 2 and Table 1, it showed that the addition of different concentrations of $NaBF_4$ has less significant effect to the morphology of TNTAs,**a**, TNTAs,**b**, TNTAs,**c** and it is predicted since the $NaBF_4$ addition is only in a small amount.

The elemental composition of these synthesized photocatalysts was estimated by EDAX analysis as presented in Fig. 4 and Table 2. The EDAX results indicated that besides Ti and O, C, N, F, B were detected. These elements were adsorbed during the anodization process and they stayed on the surface of TNTAs. Annealing under H_2 atmosphere might also play a role in their availability in the TNTAs, since some precursors in the electrolyte solution decomposed. Carbon was supplied by glycerol [21], N was supplied by NH_4F [19], F was supplied by NH_4F [19] and $NaBF_4$, whereas, B was supplied by $NaBF_4$ [10]. In this analysis, Na was not detected and may be caused by its availability in a small amount. To verify the incorporation of these elements in the lattice of TNTAs, FTIR analysis was performed.

Table 1 – The inner diameter, wall thickness and length of photocatalysts.

Photocatalyst	ID[a] (nm)	t^b (nm)	L^c (μm)
TNTAs	74–120	27	1.51
TNTAs,a	62–123	26	1.47
TNTAs,b	67–126	26	1.58
TNTAs,c	64–130	29	1.56

[a] Range inner diameter.
[b] Average wall thickness.
[c] Average length of tube.

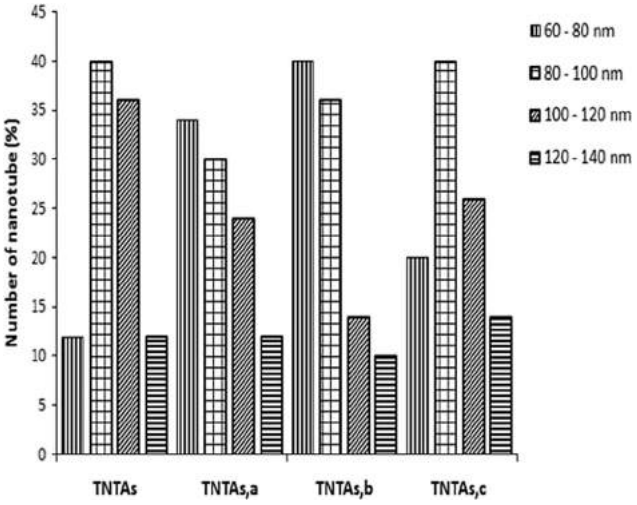

Fig. 3 – Distribution of the inner diameter in various photocatalysts.

FTIR analysis

The functional groups that present in synthesized photocatalysts can be determined by FTIR as shown in Fig. 5. The transmission peaks observed at 420 and 840 cm^{-1} correspond to the Ti–O–Ti stretching vibrations of crystalline TiO_2 [24,25]. The peaks at 1046 cm^{-1} are assigned for N–Ti–O bond

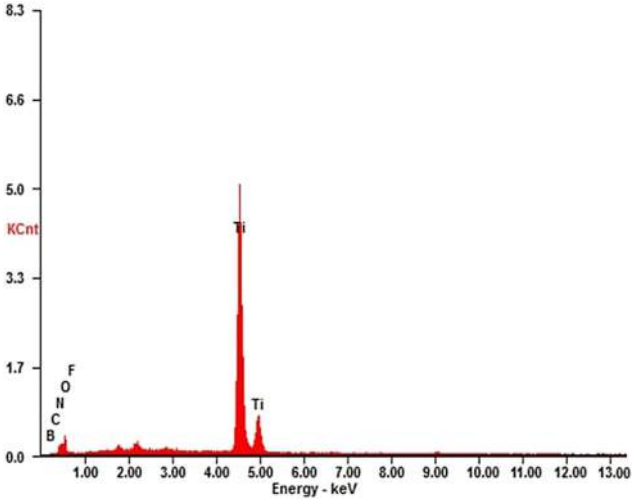

Fig. 4 – EDAX analysis of the TNTA,c.

Table 2 – Elemental composition of the photocatalysts.

Component	Wt.%			
	TNTAs	TNTAs,a	TNTAs,b	TNTAs,c
Ti	55.58	63.71	64.26	60.53
O	33.84	26.70	26.10	29.48
B	–	0.59	0.81	0.84
C	1.58	1.12	1.21	1.31
N	7.19	6.00	5.43	6.41
F	2.14	1.95	2.18	1.45

(substitutional N doping in the TNTAs) [25], whereas a small peak at around 1200 cm^{-1} is possibly for Ti–O–C bond (interstitial C doping in the lattice of TNTAs) [26,27]. When TNTAs were annealed by H_2/Ar, unsaturated titanium cation such as Ti^{3+} was generated [17]. Consequently, O_2 was liberated from TNTAs and it causes O_2 vacancy that will be substituted by Nitrogen to form N–Ti–O bond. This result was also evidenced by EDAX analysis (Table 2) as all photocatalysts contain C and N elements. For the TNTAs,**a**, TNTAs,**b** and TNTAs,**c**, a distinct peak around 1276 cm^{-1} is attributed to asymmetric stretching of the B–O vibration (Ti–O–B bond or interstitial B doping in the lattice of TNT) [24,28]. Furthermore, a distinct peak around 1560 cm^{-1} (inset as TNTAs,**a**) is attributed to the bending vibration of surface hydroxyl (surface adsorbed water molecules) [25]. Meanwhile, only weak peak is observed for the TNTAs at that wavenumber (inset as TNTAs). For all photocatalysts, a small peak at around 3700 cm^{-1} which is assigned as O–H stretching of the hydroxyl group to Ti atoms was observed. The existence of Ti–O–C, N–Ti–O or Ti–O–B bonds characterized by FTIR suggests that C, N and B were already doped in the matrix of TNTAs. The presence of F is not clearly identified by the FTIR analysis [28]. When annealing of amorphous TNTAs at 500 °C for 3 h under 20% H_2 in argon atmosphere, glycerol, NH_4F and $NaBF_4$ presence in the electrolyte solution possibly decomposed, it leads to the internal diffusion of C, N, F and B into TNTAs lattice. Those non-metals can substitute or only be adsorbed and bonded to oxygen atoms in TNTAs. Anodic oxidation in organic electrolytes such as glycerol [21] and ethylene glycol [14,18,21] could result in the incorporation of carbon into the TNTAs.

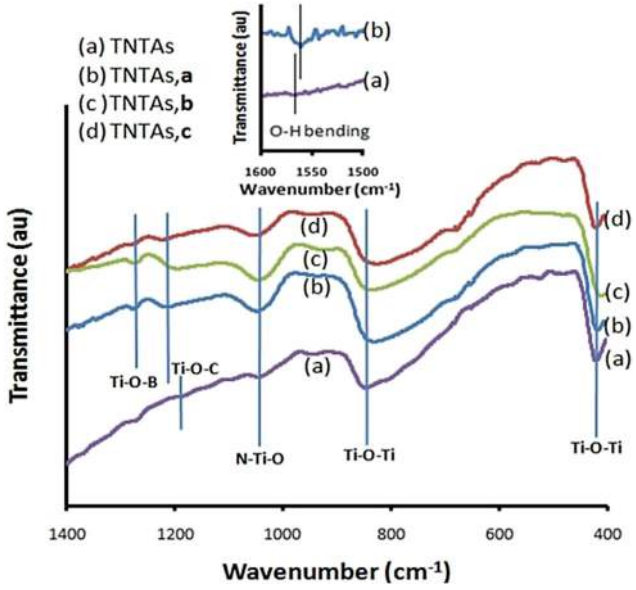

Fig. 5 – FTIR spectra of (a) TNTAs, (b) TNTAs,a, (c) TNTAs,b and (d) TNTAs,c.

UV–Vis DRS spectra analysis

Fig. 6 shows the UV–Vis absorption spectra of as prepared photocatalysts. DRS spectra data were presented with the aim to see the effect of $NaBF_4$ addition to the photocatalyst band gap. The band gap energies of TiO_2 P25 film, TNTAs and TNTAs,**a**, TNTAs,**b** TNTAs,**c** are estimated with the Kubelka–Munk function and Tauc plot [9,29] and the calculation result is presented in the Table in Fig. 6 inset. These results suggest that all photocatalysts exhibit enhancement in photoresponse under visible light as shown in Fig. 6. Compared to the TiO_2 P25 film (3.28 eV, 380 nm), reducing the band gap of TNTAs, down to 2.7 eV is caused by incorporating dopant C and N to form Ti–O–C and Ti–N–O bonds as previously explained in FTIR analysis, and substitutional N doping has more influence than that of interstitial C doping. The availability of dopant F is also predicted in reducing the band gap of TNTAs although it is not clearly identified by FTIR. After $NaBF_4$ addition to the TNTAs, the absorption band edge of all photocatalysts showed a slight blue-shift (around 3.0 eV, 410 nm) compared to that of TNTAs (2.7 eV, 460 nm). This increasing band gap may be attributed to interstitial B doping (Ti–O–B) in the TNTAs,**a**, TNTAs,**b** and TNTAs,**c** [30]. The band gap of B doped TiO_2 wider than that of un-doped TiO_2 is also reported by other researchers [31,32]. The small blue-shift may be attributed to the interstitial B doping (Ti–O–B), while substitutional B doping (B–Ti–O) would lead to the red-shift [9,30]. On the other hand, the absorption band edge showed a slight red-shift after boron doping as previously reported by other researchers [10,20]. This phenomenon is explained by investigations of different doping process. However, the optical mechanism is still not clear at present [30]. Since all photocatalysts undergo reducing the band gap compared to TiO_2 P25, they might show enhanced photoresponse under visible

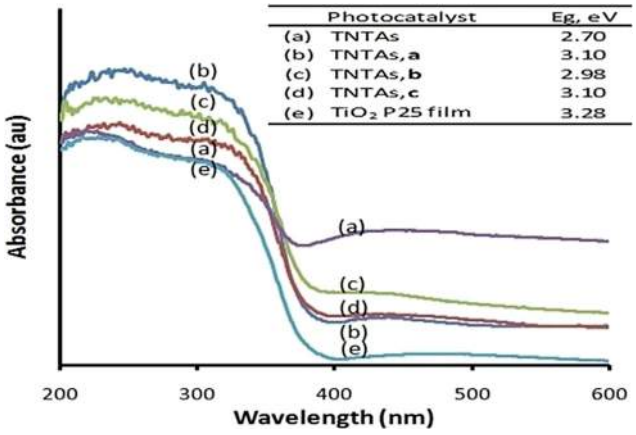

Fig. 6 – DRS spectra of (a) TNTAs, (b) TNTAs,a, (c) TNTAs,b and (d) TNTAs,c and (e) TiO_2 P25 film.

light and could be activated by visible light as well. According to Fig. 6(a and e), the increasing absorption of TNTAs after 380 nm is caused by the dopant C, N and F. For all TNTAs,**a**, TNTAs,**b**, and TNTAs,**c**, band gap energies of these photocatalysts increase, therefore, the absorptions after band edge decrease (Fig. 6(b–d)). The increasing absorption after 380 nm for all photocatalysts is proportional to the band gap values.

XRD pattern analysis

Fig. 7 shows the effect of different amount of $NaBF_4$ addition on the crystal structure and crystallite size of the photocatalyst. Annealing the photocatalyst under 20% H_2 in argon atmosphere at 500 °C for 3 h, TNTAs and TNTAs,**b** have 100% anatase phase which corresponding to $2\theta = 25.4°$ (Fig. 7(a and b)) according to JCPDS no. 21-1272. Meanwhile, very little amount of rutile phase (10%) which corresponding to $2\theta = 27.5°$ with crystallite size of 19 nm was obtained for the TNTAs,**c** (JCPDS no.21-1276). Anatase crystallite size for TNTAs, TNTAs,**b** and TNTAs,**c** calculated by Debye–Scherrer equation [19] are 22, 18 and 20 nm, respectively. The anatase and rutile crystallite size of TiO_2 P25 is 20 and 23 nm, respectively. According to Yongmei et al. [9], doping boron to the TNT via sol–gel followed by solvothermal precess could retard anatase-rutile phase transition. In addition, doping boron to TNTAs via chemical vapor deposition (CVD) also inhibits the formation of rutile phase [20]. In this study, compared to the TNTAs,**b**, the addition of $NaBF_4$ 7.5 mM to the electrolyte solution (TNTAs,**c**) causes little change of anatase to rutile phase (10%) and increases the crystallite size (20 nm). This rutile phase formation is speculated due to the availability of boron and sodium (Na). The transformation of anatase to rutile depends on the process of nucleation and growth of particle. As annealing in this study at 500 °C, the rate of transformation is limited by the rate of nucleation. It is predicted that small anatase particles tend to become bigger. As a result, transformation of anatase to rutile can be occurred

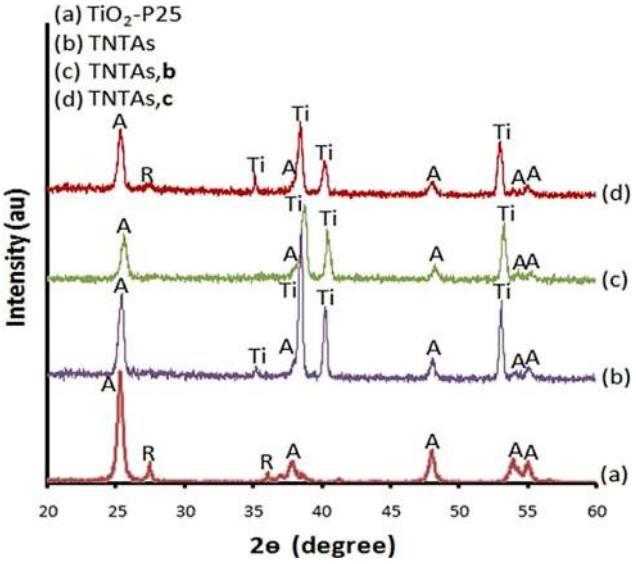

Fig. 7 – XRD spectra of (a) TiO_2 P25. (b) TNTAs, (c) TNTAs,b and (d) TNTAs,c.

and it is attributed to boron doping. Furthermore, when TiO_2 is doped with Na, the anatase and the rutile phase were observed [33]. Daimei et al. [34] reported that B-doped TiO_2 would suppress the growth of crystallite size and until a certain amount of boron, it can increase the crystallite size. The crystallite size is a crucial factor to determine the stability of photocatalyst crystalline phase. Since TNTAs,**b** has smaller crystallite size than TNTAs,**c** as shown at Table 3, TNTAs,**b** is more stable and consequently no anatase transforms to rutile phase. The C, N, F or B atoms were incorporated into the TNTAs lattice; thus the diffraction peaks were not detected due to those atoms were highly dispersed and had small content on TNTAs [31]. As these dopants were incorporated in the TNTAs lattice, the change in d-spacing was observed. Furthermore, the absence of Na titanate crystallite peak might be caused by low concentration of Na which was highly dispersed. The crystallite size of TNTAs after addition of $NaBF_4$ is lower than that of TNTAs, which may indicate the occurrence of a slight lattice distortion in the structure of TNTAs,**b** and TNTAs,**c**.

Photoelectrochemical test of photocatalyst

Fig. 8 shows the photocurrent density as a function of applied potential curves of the various photocatalysts (as photoanodes) in 0.1 M $NaNO_3$ electrolyte under UV and visible light illumination. The currents are resulted by photocatalysts with 2 cm^2 exposed area. The observed dark current was found to be negligible as it approaches zero (figure not presented). According to Fig. 8, it is clear that the photocurrents generated by TNTAs,**a**, TNTAs,**b**, TNTAs,**c** are higher than that of the TNTAs. It means that more photoexcited electrons on these photocatalysts (as photoanodes) flow to the counter electrode (Pt), leaving more holes involved in the oxidation reaction. Increasing photocurrent density of TNTAs,**a**, TNTA**s,b**, TNTAs,**c** could be attributed to the addition of $NaBF_4$ especially by dopant boron since it can suppress recombination. Boron can enhance surface acidity of TNTAs and molecules polar such as water can easy to be adsorbed on the TNTAs surface [20]. Moreover, although the existence of F is not detected by FTIR analysis (but it is detected in EDAX analysis), this anion could also enhance photocatalytic activity since it can promote surface acidity, create oxygen vacancies and increase the active site of TNTAs [35]. The availability of surface adsorbed water molecules on TNTAs,**a**, TNTA**s,b**, TNTAs,**c** identified by FTIR can trap holes to produce ·OH or active oxygen species and, therefore, recombination can be reduced [24,31]. Nianjun et al. reported that boron doping could retard the recombination of electrons and holes [31].

Table 3 – Crystallite size and anatase fraction of the photocatalysts.

Photocatalyst	Anatase crystallite size (nm)	Rutile crystallite size (nm)	Anatase fraction (wt.%)
TiO_2 P25	20	23	79
TNTAs	22	–	100
TNTAs,b	18	–	100
TNTAs,c	20	19	90

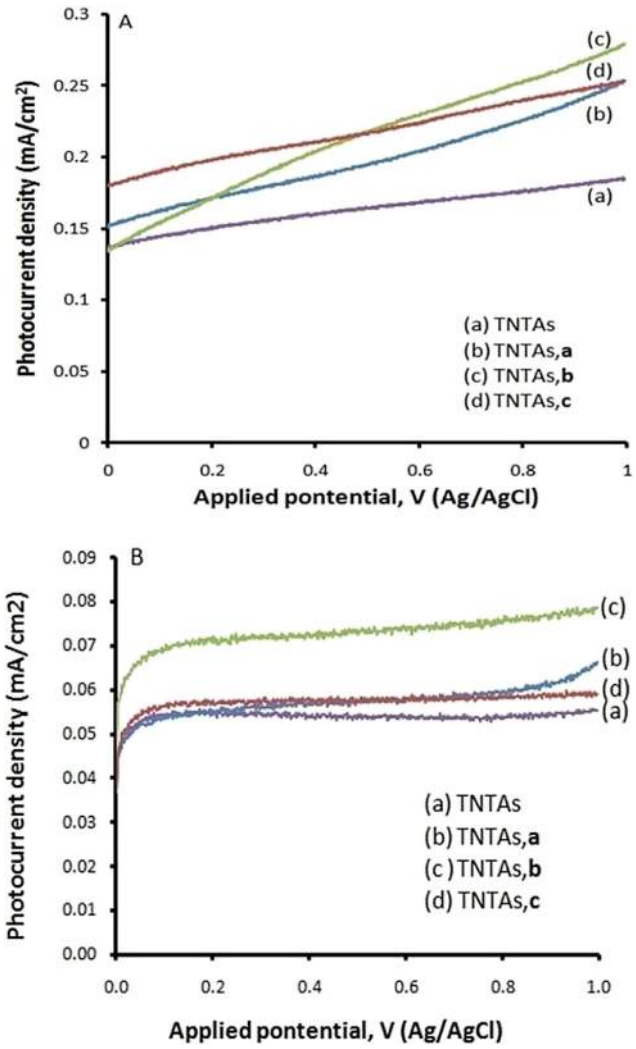

Fig. 8 – Photocurrent density vs. applied potential of different photocatalysts under illumination of: A. UV light and B. visible light.

After $NaBF_4$ addition, the surface adsorbed water molecules of TNTAs,**a,** TNTA**s,b,** TNTAs,**c** increase and % absorbance for the TNTAs,**b** is highest among others (inset in Fig. 5 as TNTAs,**a** and TNTAs). It meant that photocatalyst TNTAs,**b,** which has no rutile phase, has more surface adsorbed water molecules, thus, more recombination can be suppressed. The anatase TNTAs have higher amount of surface adsorbed water molecules than the rutile TNTAs, and therefore, anatase has higher photocatalytic activity than rutile is reported by Gang et al. [24]. This situation can enhance the photocurrent density as well as H_2 generation. Moreover, excess boron loading on TNTAs than the optimal condition could create a negative effect on photocatalytic activity, as also reported by some researchers [9,10]. This excess would become the recombination centers of the photo-induced electrons and holes. The photocurrent density of TNTAs,**b** under illumination of UV and visible light is the highest among others, which is approximately 1.5 times of TNTAs, as shown in Fig. 8. Similar results have also been reported by some researchers [10,36].

Photocatalytic test for hydrogen production

Fig. 9 shows accumulative H_2 production (μmol/cm^2 of photocatalyst) from glycerol solution as a function of irradiation time on TNTAs with various concentrations of $NaBF_4$. During the process, the temperature of the reactor was measured using a thermocouple and after 75 min irradiation the temperature was constant at about 80 °C and it is maintained with the exhaust fan. The initial pH was around 6. It is obvious that, the production of hydrogen is enhanced by addition of $NaBF_4$ on TNTAs. Fig. 9 clearly shows that, after 4 h irradiation, TNTAs,**a**, TNTA**s,b** and TNTAs,**c** can produce 5.8, 6.2 and 5.5 μmol/cm^2, respectively. Meanwhile, TNTAs only produces 4.7 μmol/cm^2. It can be stated that the TNTAs,**b** enhanced H_2 production up to 32% compare to that of TNTAs (Fig. 9(a and c)). The H_2 production enhancement could be the effect of $NaBF_4$ addition, where B and F may reduce the recombination of electrons-holes and therefore, increase the photocatalytic activity [31,35]. This phenomenon has also been occurred at B + N co-doped TiO_2, whereas boron doping could reduce the recombination and the back reaction of H_2 and O_2 into water, thereby increasing H_2 formation [31]. Surface adsorbed water molecules of TNTAs,**a**, TNTA**s,b**, TNTAs,**c** can trap holes to generate active species ·OH and H^+. Thus, recombination can be suppressed and hydrogen generation is enhanced as more H_2O can react with holes, resulting in the reaction shifted to the product. Therefore, more H_2 is produced. Furthermore, active species ·OH can react with glycerol to produce H_2 as well. According to Fig. 9(b–d), the optimal performance was achieved by TNTAs,**b**, since more recombination electron–hole can be suppressed in that sample compared to others. This condition is in agreement with the result of this study in photoelectrochemical measurement (Fig. 8) as previously reported.

Photocatalytic production of H_2 from glycerol solution (glycerol–water mixture) consists of two distinct mechanisms namely photo-spitting of water (at glycerol concentration of

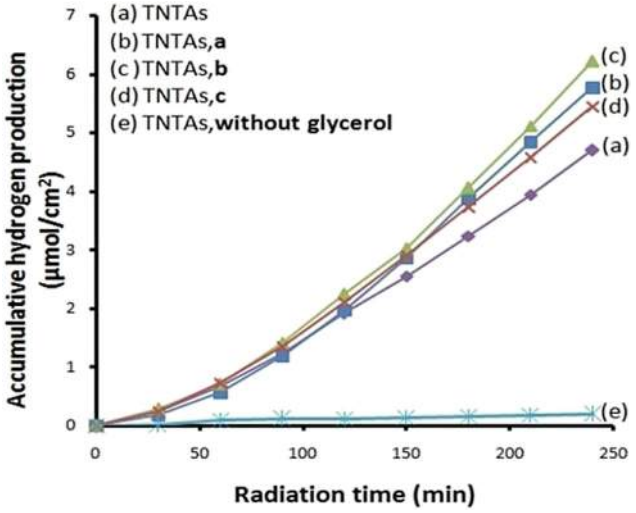

Fig. 9 – Hydrogen production of (a) TNTAs (b) TNTAs,a, (c) TNTAs,b, (d) TNTAs,c in 10% glycerol concentration and (e) TNTAs in 0% glycerol concentration.

0%) and photo-reforming of glycerol [7]. In photo-splitting of water, hole oxidizes water to produce ·OH and H^+ according to Eq. (4), then H^+ undergoes reduction with electron to produce H_2 (Eq. (5)).

$$TiO_2 + hv \rightarrow TiO_2(h^+ + e^-) \quad (3)$$

$$h^+ + H_2O \rightarrow \cdot OH + H^+ \quad (4)$$

$$H^+ + e^- \rightarrow 0.5H_2 \quad (5)$$

In photo-reforming of glycerol, it is oxidized by hole, ·OH and/or oxygen produced by cleavage of water to produce several intermediate compounds followed by H_2 and CO_2 generation as the end product [6,31]. The two reactions (photo-spitting of water and photo-reforming of glycerol) take place simultaneously, and the combination of those reactions called as glycerol steam photo-reforming according to the overall reaction as follows [6,7,31,37]:

$$C_3H_8O_3 + 3H_2O \rightarrow 3CO_2 + 7H_2 \quad (6)$$

Therefore, introducing glycerol in the reactant could improve H_2 production as glycerol can act as sacrificial agents/hole scavenger that able to reduce the electron–hole recombination and as hydrogen source/reactant that undergoes oxidation reaction [6,7]. As glycerol is also oxidized by oxygen produced by cleavage of water, O_2–H_2 back reaction can be diminished [6]. Moreover, glycerol can act as sacrificial agents/electron donor in water splitting that can enhance the H_2 production [6,7,31]. Detail mechanism of glycerol–water decomposition to produce H_2 has been proposed by Min et al. [38]. The 10% glycerol concentration in this study represents its concentration in the biodiesel waste, and it is sufficient to give a substantial improvement to the photocatalytic H_2 generation catalyzed by Pt–N-TNT [37]. In this study, small amount of CO_2 was detected, but it does not agree with the stoichiometry of the glycerol photo-reforming reaction (Eq. (6)). This condition may be due to the solubility of CO_2 in water (1.45 g/L H_2O), since the solution become acid after 4 h irradiation [31]. In addition, this study also indicated that in the absence of glycerol in the solution (water splitting process), produced hydrogen was small as only 0.2 μmol/cm^2 of H_2 was generated by TNTAs (Fig. 9(e)). This due to the high rate of recombination, backward reaction and lack of the hydrogen source. When there is no irradiation or no photocatalyst, H_2 is not obtained since there is no photon source and no photocatalyst (data not presented).

Conclusions

The $NaBF_4$ addition during the anodic synthesis of TiO_2 nanotube arrays (TNTAs) followed by annealing under 20% H_2 in argon at 500 °C for 3 h was not change the morphology of TNTAs but did enhance its photocatalytic performance. The FTIR result indicated that C, N and B were incorporated in the lattice of TNTAs to form Ti–O–C, N–Ti–O and Ti–O–B bonds. The addition of $NaBF_4$ on TNTAs can reduce the recombination and promote photocatalytic activity, therefore, it can enhance photocurrent density under UV or visible light and hydrogen production from glycerol–water mixture compare to the TNTAs. Glycerol as a sacrificial agent and hydrogen source can be used to enhance H_2 generation. The result indicated that, under current condition, the addition of 5 mM $NaBF_4$ to the electrolyte solution in the anodization process (TNTAs,**b**) exhibited the optimum photocatalyst performance.

Acknowledgments

The authors would like to thank LP3M Institut Teknologi Indonesia and Directorate General of Higher Education (DGHE) Indonesian Ministry of National Education for the financial support of this research (Hibah Bersaing grant no. 025/K3/KM/SPK/2013). Also, thanks to Dian Indriani for her assistance in the data collection.

REFERENCES

[1] York RS, Biplab S, Swomitra KM, Mano S. Single-step anodization for synthesis of hierarchical TiO_2 nanotube arrays on foil and wire substrate for enhanced photoelectrochemical water splitting. Int J Hydrogen Energy 2013;38:2062–9.
[2] Haifeng D, Xinfa D, Yingchao D, Yan Z, Stuart H. TiO_2 nanotubes coupled with nano-Cu(OH)$_2$ for highly efficient photocatalytic hydrogen production. Int J Hydrogen Energy 2013;38:2126–35.
[3] Wang WC, Liu CH, Liu CW, Chao JH, Lin CH. Effect of Pt loading order on photocatalytic activity of Pt/TiO_2 nanofiber in generation of H_2 from neat ethanol. J Phys Chem C 2009;113:13832–40.
[4] Rajini PA, Tom M, Ramesh C, Murugesan M, Arup D, Dhara S, et al. Efficient photocatalytic hydrogen generation by Pt modified TiO_2 nanotubes fabricated by rapid breakdown anodization. Int J Hydrogen Energy 2012;37:8268–76.
[5] Yagmur K, Fatih A, Ekin K, Mesut A. Hydrogen production from 2-propanol over Pt/Al_2O_3 and Ru/Al_2O_3 catalyst in supercritical water. Int J Hydrogen Energy 2013;38:7298–306.
[6] Vasileia MD, Demitris IK. Efficient production of hydrogen by photo-induced reforming of glycerol at ambient conditions. Catal Today 2009;144:75–80.
[7] Slamet Dewi T, Valentina Muhammad I. Photocatalytic hydrogen production from glycerol–water mixture over Pt–N–TiO_2 nanotube photocatalyst. Int J Energy Res 2013;37:1372–81.
[8] Fuyun P, Yingliang L, Shengang X, Jing L, Chenxu W, Shaokui C. Nanocomposite of graphene oxide with nitrogen-doped TiO_2 exhibiting enhanced photocatalytic efficiency for hydrogen evolution. Int J Hydrogen Energy 2013;38:2670–7.
[9] Yongmei W, Mingyang X, Jinlong Z, Feng C. Effective visible-active boron and carbon modified TiO_2 photocatalyst for degradation of organic pollutant. App Catal B Environ 2010;97:182–9.
[10] Na L, Huimin Z, Jingyuan L, Xie Q, Shuo C. Characterization of boron-doped TiO_2 nanotube arrays prepared by electrochemical method and its visible light activity. Sep Purif Technol 2008;62:668–73.

[11] Alagesan S, Hong WW. Effects of boron doping in TiO_2 nanotubes and the performance of dye-sensitized solar cells. App Surf Sci 2012;258:6479–84.
[12] Valentina G, Laura S, Tiziano M, Juan JD, Andrzej A, Gianpiero A, et al. CuO_x–TiO_2 photocatalyst for H_2 production from ethanol and glycerol solutions. J Phys Chem A 2009;114:3916–25.
[13] Xi P, Qin X, Wu-lin C, Gui-lin Z, Xing Z, Jian-guo W. Tuning the catalytic property of TiO_2 nanotube arrays for water splitting. Int J Hydrogen Energy 2013;38:2095–105.
[14] Susanta KM, Mano M, Vishal KM, Krishnan SR. Design of a highly efficient photocatalytic cell for hydrogen generation by water splitting: application of $TiO_{2-x}C_x$ nanotube as a photoanode and Pt/TiO_2 nanotube as a cathode. J Phys Chem C 2007;111:8677–85.
[15] Li CL, Yuan J, Han BY, Jiang L, Shangguan WF. TiO_2 nanotubes incorporated with CdS for photocatalytic hydrogen production from spitting of water under visible light irradiation. Int J Hydrogen Energy 2013;38:7298–306.
[16] Muhamed AER, Rohani S. Modified TiO_2 nanotube arrays (TNTAs): progressive strategies towards visible light responsive photoanode, a review. Energy Environ Sci 2011;4:1065–86.
[17] Poulomi R, Steffen B, Patric S. TiO_2 nanotube: synthesis and applications. Angew Chem Int Ed 2011;50:2904–39.
[18] Susanta KM, Mano M, Vishal KM, Krishnan SR. A novel method for the synthesis of titania nanotube using sonoelectrochemical method and its application for photoelectrochemical splitting of water. J Catal 2007;246:362–9.
[19] Hongjun W, Zhonghai Z. High photoelectrochemical water splitting performance on nitrogen doped double wall TiO_2 nanotube arrays electrode. Int J Hydrogen Energy 2011;36:13481–7.
[20] Yaling S, Song H, Xingwang Z, Xiuqin C, Lecheng L. Preparation and visible-light-driven photoelectrocatalytic properties of boron-doped TiO_2 nanotubes. Mat Chem Phys 2006;110:239–46.
[21] Fathy MBH, Hiroshi N, Shanmugam V, Mitsuhiro K, Takeo E. Functionalization of electrochemically prepared titania nanotubes with Pt for application as catalyst for fuel cells. J Power Sources 2010;195:5889–95.
[22] Sorachon Y. Effect of inter-electrode spacing on electrolyte properties and morphologies of anodic TiO_2 nanotube array films. Int J Electrochem Sci 2012;7:9454–64.
[23] Wen YW, Ruei CB. Characterization and photocatalytic activity of TiO_2 nanotube film prepared by anodization. Int J Photoenergy 2013:1–12.
[24] Gang L, Chenghua S, Lina C, Yonggang J, Haofeng L, Lianzhou W, et al. Efficient promotion of anatase TiO_2 photocatalyst via bifunctional surface-terminating Ti–O–B–N structures. J Phys Chem C 2009;113:12317–24.
[25] Yean LP, Ahmad ZA. Effect of carbon and nitrogen co-doping on characteristics and sonocatalytic activity of TiO_2 nanotube TNT for degradation of Rhodamine B in water. Chem Eng J 2013;214:129–38.
[26] Parra R, Goes MS, Castro MS, Longo E, Bueno PR, Varela JA. Reaction pathway to the synthesis of anatase via the chemical modification of titanium isopropoxide with acetic acid. Chem Mater 2008;20:143–50.
[27] Sadiye S, Murat E, Meltem A, Hikmet S. The effect of silane modification on the adsorptive properties of natural pirophyllite and synthetic titanium-based powders prepared by the sol–gel process. Turk J Chem 2005;29:487–95.
[28] Young-Seak L, Sang JK, Venkateswaran P, Jeen-Seok J, Hyuk K, Jong-Gyu K. Anion co-doped titania for solar photocatalytic degradation of dyes. Carbon Lett 2008;9:131–6.
[29] Liu X, Liu Z, Zheng J, Yan X, Li D, Chen S, et al. Characteristics of N-doped TiO_2 nanotube arrays by N_2-plasma for visible light-driven photocatalysis. J Alloys Compd 2011;509:9970–6.
[30] Guo ML, Xiao DZ, Liang CT. Concentration-dependent electronic structure and optical absorption properties of B-doped anatase TiO_2. Phys B 2011;406:3354–8.
[31] Nianjun L, Zheng J, Huahong S, Fahai C, Tiancun X, Peter PE. Photo-catalytic conversion of oxygenated hydrocarbons to hydrogen over heteroatom-doped TiO_2 catalyst. Int J Hydrogen Energy 2009;34:125–9.
[32] Xing D, Xiao S, Pengna L, Zhihui A, Lizhi Z. Efficient visible light driven photocatalytic removal of NO with aerosol flow synthesized B, N-codoped TiO_2 hollow spheres. J Hazard Mater 2011;190:604–12.
[33] Zamora T, Lopez T, Gomez R, Azomoza M, Melendrez R. Oligomerization of acetone over titania-doped catalysts (Li, Na, K and Cs): effect of alkaline metal in activity and selectivity. Catal Today 2005;107–108:289–93.
[34] Daimei C, Dong Y, Qun W, Zhongyi J. Effects of boron doping on photocatalytic activity and microstructure of titanium dioxide nanoparticles. Ind Eng Chem Res 2006;45:4110–6.
[35] Di L, Hajime H, Shunichi H, Naoki O, Nitin KL. Fluorine-doped TiO_2 powders prepared by spray pyrolysis and their improved photocatalyic activity for decomposition of gas-phase acetaldehyde. J Fluor Chem 2005;126:69–77.
[36] Na L, Xie Q, Jing YL, Shuo C, Hong TY, Guo HC. Fabrication of boron-doped TiO_2 nanotube array electrode and investigation of its photoelectrochemical capability. J Phys Chem C 2007;111:11836–42.
[37] Slamet, Eny K, Agus FA, Setiadi. Photocatalytic reforming of glycerol–water over nitrogen and nickel- doped titanium dioxide nanoparticles. Int J Eng Tech 2012;12:47–53.
[38] Min L, Yuexiang L, Shaoqin P, Gongxuan L, Shuben L. Photocatalytic hydrogen generation using glycerol wastewater over Pt/TiO_2. Front Chem China 2009;4:32–8.